Stress inversion of earthquake focal mechanism solutions from onshore and offshore Norway

ERIK C. HICKS, HILMAR BUNGUM & CONRAD D. LINDHOLM

A comprehensive compilation of 112 earthquake focal mechanism solutions in Norway and adjacent areas has been completed, including 7 previously unpublished solutions for recent earthquakes determined as part of the NEONOR (Neotectonics in Norway) project. Using the method of Gephart & Forsyth (1984), the 97 solutions on the Norwegian mainland and margin have been inverted with respect to primary stress directions, which on a regional basis and in the best possible way could satisfy the individual solutions. In doing this the Norwegian mainland and margin areas were divided into six zones containing between 5 and 34 earthquake focal mechanism solutions. Two additional zones containing only in situ measurements are also defined, and horizontal stress directions evaluated. The results show a tendency for oblique-slip reverse faulting offshore, for oblique-slip normal faulting onshore and for average stress directions which are in overall compliance with a NW–SE oriented regional stress field assumed to be dominated by the mid-Atlantic ridge-push force. Local variations do exist, however, in particular for more shallow earthquakes in mid-Norway coastal areas, where the dominating compressive stress directions are NE–SW, implying coast-perpendicular extension. While this may be related to different kinds of local effects, it is also possible that deglaciation flexure can explain the observed stress directions in this region, since this is also where we find the maximum postglacial uplift gradients.

Erik C. Hicks, NORSAR, P.O. Box 51, N-2027 Kjeller, Norway

Introduction

Earthquakes contribute essentially in two different ways to the understanding of the seismotectonic conditions in any particular region, firstly through analysis of individual earthquakes (single sources), such as location, size, mode of faulting, rupture characteristics, etc., and the way the event may fit into the seismic cycle, and, secondly, through various ensemble analyses, essentially spatio-temporal characteristics as expressed through recurrence behaviour, seismic lineations, etc. Both types of analysis are important when the goal is to improve our understanding of lithospheric seismo-dynamics, provided that such information is properly tied in to structural geologic and geodetic observations.

The earthquake activity in and around Norway has been documented through a number of detailed studies, and for comprehensive analyses and reviews here we refer to Bungum et al. (1991) and to Byrkjeland et al. (2000). It is concluded there that while the stress field along the margin is generally consistent with the ridge-push force, regional and local stress enhancement factors (such as sedimentary loading and topography) are also essential for explaining the earthquake activity along and near the Norwegian continental margin. The potential for earthquake occurrence, including structural reactivation, is therefore most likely tied to a mixture of platewide, regional and local stress, in combination with existing weakness zones and faults, without any single factor being dominant.

The purpose of the present paper is twofold, firstly to provide a comprehensive and consistent overview of all available earthquake focal mechanism solutions for both onshore and offshore Norway, including some new and unpublished solutions, and, secondly, to analyse these solutions in search for regionally consistent stress patterns using the stress inversion method of Gephart & Forsyth (1984). Six regions are covered in this way (Northern North Sea, Offshore Mid Norway, Onshore Mid Norway, Onshore West Norway, Oslo Rift Zone and Finnmark) and in addition we have covered two more regions using in situ stress data (Western Barents Sea and Southern North Sea).

Earthquake focal mechanisms

First motion polarities

The classical and most widely used method for determining an earthquake focal mechanism solution is to use P-wave first-motion polarities in sampling sense of motion in different ray directions from the source, thereby defining the two nodal planes, delineated in a (usually lower hemisphere) stereographic plot. To do this with sufficient precision, a good station coverage of azimuths and distances is needed, a condition which quite often is not met when analysing the seismicity in and around Norway. However, some earthquakes are located close to or within denser local networks, and many of the larger earthquakes also have an adequate signal-to-noise ratio to allow first-motion determination at a sufficient number of stations for a solution to be determined in this manner. Four of the seven new earthquake focal mechanism solutions published for the first time in this paper were determined using first-motion polarities only, as these were located close to
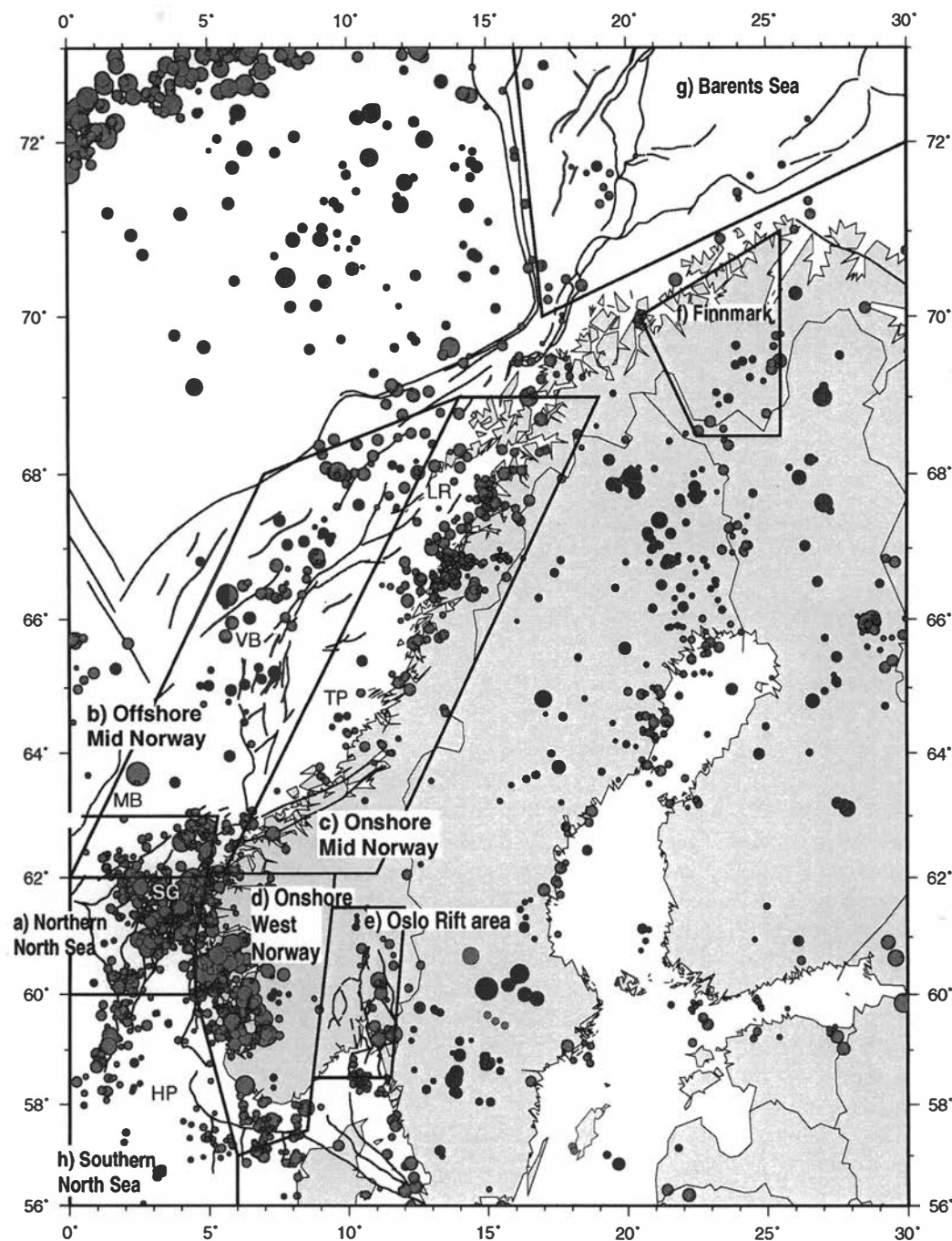
Fig. 1. Earthquakes in Norway and surrounding areas for the time period 1980–1999, magnitudes greater than or equal to 2.0 (symbol size proportional to magnitude). Note the areas of higher seismic activity in the northern North Sea and onshore in western Norway, separated by the Horda Platform (HP) but coming together in the Sogn Graben (SG) area. In northern Norway there is a similar separation in that a more or less aseismic Vøring Shelf (Trøndelag Platform – TP) is separating the seismic activity along the continental margin in the Møre (MB) and Vøring (VB) basins from that along the Nordland coast, coming together in the Lofoten region (LR). The Oslo rift appears to have a higher level of seismic activity than the surrounding basement. The zones (with names) used in the stress inversion are shown. Note that the Northern North Sea and Offshore Mid-Norway zones overlap around 62–63° N. Focal mechanism solutions in the overlapping area have been used in the inversions from both areas.

temporary local seismic networks in western and mid-Norway operated under the Neotectonics in Norway (NEONOR) project (Dehls & Olesen 1998, 1999, 2000; Hicks et al. 2000). In addition, these earthquakes were of sufficiently large magnitude to also have identifiable first-motion polarities at several of the permanent stations within the Norwegian seismic network, giving a coverage sufficient to allow for reasonably reliable focal mechanism solutions. The actual solutions are developed by performing a simple grid search, allowing for a systematic comparison between data and model. The remaining three new solutions are also located close to the same local networks, so the location accuracies for the epicentres are therefore better than generally available from the perma-

nent national network in these areas, better than 5 km for the 1999.04.09 event, and better than 10 km for the other 6 earthquakes.

Waveform modelling

For earthquakes that do not have a large enough number of available first-motion polarities, it is possible to use full waveform modelling to select (constrain) a focal mechanism solution, or at least to support indications from first-motion data. This is the case for the other three of the seven new mechanisms. One of the earthquakes was close to the temporary network in mid-Norway, but since the permanent Norwegian network has few stations in this area the
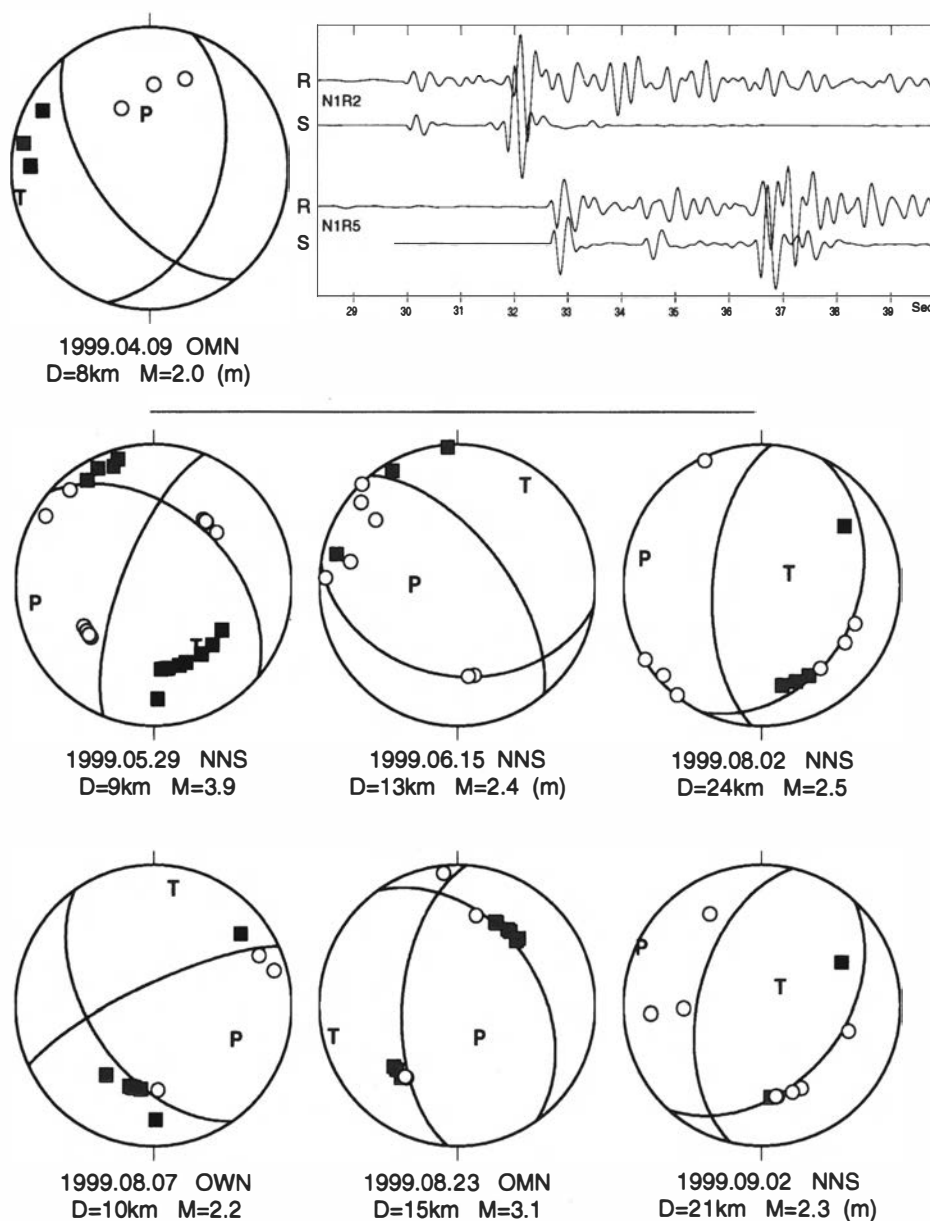
Fig. 2. Seven previously unpublished earthquake focal mechanism solutions with available first-motion polarities used in this study are shown. Full-waveform modelling examples are shown for the 1999.04.09 solution for stations at 13 and 31 km distance (R-real, S-synthetic data). Solutions determined through waveform modelling are marked (m). NNS – Northern North Sea, OWN – Onshore West Norway, OMN – Onshore Mid-Norway. The 1999.04.09 and 1999.08.23 solutions from onshore mid-Norway both show a clear rotation (E–W tension) compared to the solutions from western Norway, which comply fairly well with the expected WNW–ESE compression of the 'ridge push' force.

available first motions were only able to provide a rough constraint on the focal mechanism solution. The final two earthquakes were located close to the network in western Norway, but first motions alone were insufficient to determine a solution with sufficient precision.

After reading all available first-motion polarities for these three earthquakes, possible focal mechanism solutions were determined using the same grid search method as used in the first-motion only determinations. Subsequently, synthetic seismograms for the possible focal mechanism solutions were generated for selected stations with good data quality, using the Herrmann code (e.g. Herrmann 1978, 1979; Wang & Herrmann 1980). The algorithm uses discrete wavenumber integration to consider the complete wave field of a point source, which is quite computer-time-consuming. However, once this step has been performed for an earthquake location and defined stations, the actual synthetic seismogram for various

source focal mechanisms can be generated much more quickly. In comparing synthetic seismograms for the possible focal mechanism solutions with observed data, the main emphasis is on the relative amplitudes for the P and S phases, whereupon the solution giving the best correlation based on a visual judgement for the modelled stations is selected. Given that the earlier data only consist of one available focal mechanism solution, we have elected to select and use a single "best" solution for each new earthquake in order to avoid weighting problems, as opposed to using a range of acceptable solutions for each event as input to the inversion, as used by for example Lund & Slunga (1999).

New solutions

The seven new earthquake focal mechanism solutions are shown in Fig. 2, with available first-motion polarities. It
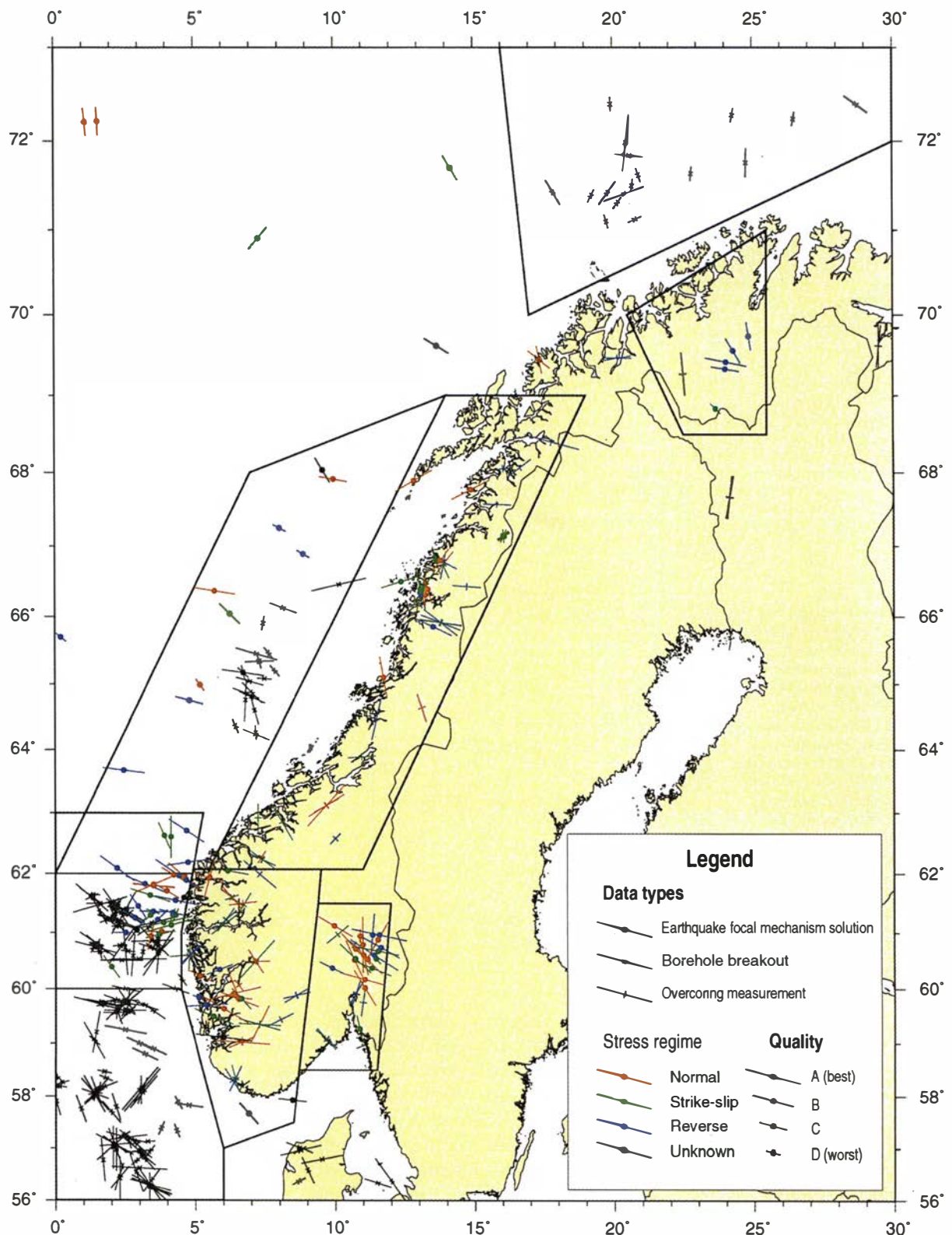
Fig. 3. Directions of maximum horizontal compressive stress and stress regime by color for the individual data. Circles represent earthquake focal mechanism solutions, crossbars are overcoring measurements and crosses are borehole breakouts. The length of the bars reflect the World Stress Map (WSM) quality rating of the data (Zoback et al. 1992).

can be seen there that the solution for the 99.04.09 earthquake is not very well resolved from the first-motion data, so in that case we have also used full-waveform modelling to further constrain the solution, for two stations as also shown in Fig. 3 (at 13 and 31 km distance) and for two more stations not shown, with distances up to 60 km. The 99.06.15 earthquake is better resolved from polarities and it is of slightly larger magnitude but observed at

Table 1. Complete list of earthquake focal mechanism solutions in Norway.

Date	Lat	Lon	Depth	Mag	T-trn	T-plg	P-trn	P-plg	Ref.	Com.	Qual	σ_H	Reg.
Com.–78	66.80	13.65	9	−1.0	258	11	164	18	6		C	164	SS
Com.–78	66.80	13.80	6	−1.0	132	15	255	64	5		C	36	NF
Com.–81	77.70	17.00	4	−1.0	315	90	270	0	8		?	270	TF
Com.–82	80.20	21.70	4	−1.0	15	0	285	0	9		B	285	SS
Com.–82	80.10	20.00	4	−1.0	187	45	298	20	9		B	298	TS
Com.–82	80.30	20.00	4	−1.0	180	0	270	0	9		B	270	SS
Com.–86	61.00	2.50	19	−1.0	270	65	90	25	12		?	90	TF
Com.–92	67.77	14.88	10	−1.0	337	6	77	55	19		B	243	NF
Com.–97	66.31	13.25	5	−1.0	270	11	167	48	21		C	0	NS
1959.01.29	70.90	7.30	33	5.8	310	20	220	10	1		?	220	SS
1959.03.01	74.80	8.10	33	5.4	120	0	25	30	1		?	210	SS
1968.01.03	72.22	1.55	33	5.2	86	1	354	46	2		C	176	NS
1970.10.21	74.62	8.56	33	5.5	82	3	349	39	2		D	172	SS
1971.05.31	72.21	1.09	20	5.5	264	1	356	49	2		C	354	NS
1971.07.19	60.72	10.73	31	1.4	227	11	127	42	3		B	317	NS
1973.11.23	60.55	11.47	23	1.7	229	3	137	26	3		D	319	SS
1975.01.20	71.70	14.20	24	5.0	59	14	156	25	2		C	149	SS
1976.01.18	77.79	18.34	4	5.5	333	9	243	2	4		?	243	SS
1977.12.11	60.94	10.89	22	2.0	95	25	259	64	3		D	2	NF
1979.03.29	60.79	10.99	11	2.2	86	13	320	69	13		A	180	NF
1979.06.14	60.38	11.32	17	2.7	204	9	113	12	7		B	113	SS
1980.11.18	60.96	11.34	30	2.2	37	53	185	32	7		B	185	TF
1981.06.22	65.70	0.20	15	4.0	161	55	309	31	13		D	309	TF
1981.06.07	60.54	11.16	19	1.3	227	10	125	49	7		B	317	NS
1981.09.03	69.62	13.68	12	4.7	49	38	301	22	13	m	C	301	U
1982.07.29	60.40	2.00	17	4.3	55	12	320	25	10		C	145	SS
1982.10.18	60.96	11.58	20	2.1	218	80	102	4	13		A	102	TF
1983.03.08	59.70	5.40	15	4.6	6	46	267	9	10		B	267	TS
1983.03.08	60.53	10.69	15	1.4	246	4	340	44	7		B	336	NS
1984.03.01	60.55	10.73	17	0.7	46	12	313	15	7		B	313.	SS
1985.01.25	61.22	3.65	33	3.1	295	45	46	20	15		C	46	TS
1985.05.16	60.94	3.41	33	2.5	104	3	205	74	15		C	13	NF
1985.09.08	61.30	3.40	19	3.1	319	8	227	14	10		D	227	SS
1985.10.01	61.30	4.20	15	3.0	109	8	200	9	10		D	200.	SS
1985.10.27	61.30	4.30	15	2.8	293	12	30	32	10		D	203	SS
1985.11.30	61.60	4.60	6	3.0	99	28	212	36	10		D	212	U
1986.02.05	62.71	4.69	20	4.9	198	55	303	10	11	m	B	303	TF
1986.10.26	61.83	3.20	14	4.5	305	78	112	12	13	m	B	112	TF
1986.12.16	60.61	11.02	11	1.9	69	30	281	56	13		B	168	NF
1987.04.04	67.25	8.03	15	3.6	17	75	118	3	13		D	118	TF
1987.09.04	61.45	2.95	33	3.0	213	69	326	9	15		C	326	TF
1987.10.31	61.13	4.14	20	3.4	345	12	248	32	13		A	255	SS
1987.12.26	59.81	6.55	12	2.4	21	4	286	47	13	m	B	111	NS
1988.01.31	68.03	9.58	20	4.3	92	24	329	51	13		C	329	U
1988.06.30	61.12	9.97	20	1.9	36	21	176	64	13		B	300	NF
1988.06.02	62.09	2.20	29	3.1	37	64	306	1	13		B	306	TF
1988.08.08	63.68	2.44	25	5.3	31	77	277	5	11		B	277	TF
1988.10.27	66.89	8.88	25	3.9	191	83	300	2	13		D	300	TF
1988.10.20	59.91	6.36	11	3.5	166	14	273	49	13		A	256	NS
1989.01.20	57.93	8.46	29	3.1	216	28	96	43	13		C	96	U
1989.01.23	61.97	4.42	26	5.1	239	72	124	8	11	m	A	124	TF
1989.01.29	59.64	6.02	7	4.2	201	15	90	54	13		A	301	NF
1989.01.09	69.56	24.30	12	1.4	182	71	329	16	14	m	C	329	TF
1989.02.14	61.17	3.87	11	2.9	348	4	81	31	13	m	A	258	SS
1989.04.10	60.61	11.40	22	1.9	35	42	303	3	13		A	303	TS
1989.07.13	69.74	24.87	8	2.1	245	52	351	12	14	m	C	351	TF
1989.09.01	61.34	4.20	33	2.6	340	63	103	16	16		C	103	TF
1989.09.02	61.36	3.49	33	2.2	16	35	109	5	16		D	109	SS
1989.09.02	61.36	3.49	33	2.5	359	48	92	3	16		C	92	TS
1989.09.20	59.11	6.01	10	2.7	210	24	97	41	13		A	97	U
1989.11.02	60.68	11.54	33	1.3	20	35	281	12	13		B	281	SS
1989.11.16	68.83	23.67	12.5	1.6	45	0	135	0	14		D	135	SS
1990.02.26	57.67	6.91	6.4	3.4	252	39	139	26	18		C	139	U
1990.05.16	66.04	6.26	30	3.4	225	1	135	10	18		C	135	SS
1991.04.13	69.33	24.02	9.7	1.8	19	69	279	4	14	m	C	279	TF
1991.09.01	79.02	3.59	10	5.0	84	0	174	0	17		C	174	SS
1991.12.31	61.98	4.23	15	3.3	210	5	30	85	17		C	120	NF
1991.12.16	67.91	9.97	10	2.4	193	5	291	60	18		C	100	NF
1992.02.19	59.27	10.88	10	3.6	258	9	160	39	18		C	348	SS
1992.04.14	59.50	5.66	12	3.0	202	30	292	0	18		B	292	SS
1992.06.30	60.88	11.53	12	2.8	299	5	182	78	18		B	30	NF
1992.08.14	67.89	12.85	17	3.7	159	23	293	58	18	m	B	60	NF
1993.01.20	64.75	4.81	15	3.5	175	90	285	0	17		C	285	TF

Table 1. Continued.

Date	Lat	Lon	Depth	Mag	T-trn	T-plg	P-trn	P-plg	Ref.	Com.	Qual	σ_H	Reg.
1993.06.26	62.61	4.14	17	3.9	280	37	180	12	18		B	180	SS
1993.09.13	66.37	5.72	20	3.9	7	9	246	72	18		B	99	NF
1993.10.18	64.99	5.19	10	3.3	49	10	299	62	18		D	144	NF
1993.12.27	61.25	2.84	20	3.3	0	58	121	18	18		?	121	TF
1994.07.27	62.63	3.90	10	3.7	66	2	334	30	17		C	156	SS
1994.08.01	60.38	9.89	5	2.1	6	57	117	13	18		C	117	TF
1994.11.19	60.17	11.06	13	3.5	185	18	68	54	18		B	286	NF
1995.02.06	59.84	6.51	10	3.0	6	19	115	44	18		?	96	NS
1995.06.20	61.71	3.98	10	2.9	31	0	300	40	18	m	C	300	NS
1995.11.13	60.02	11.06	18	3.4	239	12	343	47	18	m	B	329	NS
1996.01.21	69.42	24.04	10	4.2	25	70	281	5	18		B	281	TF
1996.02.08	61.05	2.9	·24	2.7	277	52	37	21	20		C	37	TF
1996.03.03	60.74	11.64	32	1.9	62	58	299	19	18		B	299	TF
1996.03.17	60.23	5.18	7	2.4	26	16	281	42	20		C	116	NS
1996.04.16	61.94	5.52	13	2.8	105	24	312	63	20		B	15	NF
1996.06.07	59.84	5.13	12	1.9	172	79	289	5	20		D	289	TF
1996.06.25	61.64	3.39	17	3.2	192	12	288	27	20		B	288	SS
1996.10.31	61.80	3.51	15	3.9	184	3	276	40	20		B	94	NS
1996.10.31	61.82	3.51	15	3.9	157	19	266	44	20		B	67	NS
1996.10.31	61.80	3.52	15	3.7	6	3	273	40	20		B	96	NS
1996.12.16	61.02	3.79	20	3.0	180	0	270	60	20		C	90	NF
1997.05.13	60.97	3.72	19	3.1	346	2	254	30	20		C	76	SS
1997.11.21	66.41	13.22	7	2.3	302	7	208	29	21	m	B	212	SS
1997.11.25	66.50	12.40	11	2.7	343	7	77	29	21	m	B	73	SS
1997.11.28	66.32	13.14	11	1.7	299	23	74	58	21	m	C	200	NF
1997.11.28	66.32	13.15	11	1.8	299	23	74	58	21	m	C	200	NF
1997.12.08	59.82	6.65	12	2.7	43	29	137	7	20		C	137	SS
1997.12.26	66.32	13.11	11	1.8	268	67	176	1	21	m	C	176	TF
1998.01.08	66.37	13.13	13	2.2	284	19	27	33	21	m	B	14	SS
1998.02.03	66.39	13.09	11	2.8	257	11	351	22	21	m	B	347	SS
1998.03.09	65.85	13.53	7	2.8	225	57	115	13	21	m	B	115	TF
1998.11.28	60.35	5.867	10	2.8	358	57	248	13	20		C	248	TF
1999.04.09	66.39	13.35	8	2	258	6	357	58	22	m	C	164	NF
1999.05.29	62.19	4.74	9	3.9	144	46	262	15	22		B	262	TS
1999.06.15	61.95	4.62	13	2.4	35	14	272	65	22	m	B	130	NF
1999.08.02	61.55	4.29	24	2.5	67	72	283	15	22		B	282	TF
1999.08.07	62.05	6.17	10	2.2	10	16	111	36	22		B	100	SS
1999.08.23	65.10	11.75	15	3.1	257	9	143	68	22		B	350	NF
1999.09.02	61.89	4.68	21	2.3	45	74	296	5	22	m	C	296	TF

T-trn, T-plg, P-trn and P-plg are trend and plunge for the T (tension) and P (compression) axes, respectively. An 'm' in the comment field refers to a waveform modelling approach used in determining the solution. σ_H directions according to Slunga (1981). Quality ratings and stress regime are determined according to the criteria defined in the World Stress Map project (e.g. Zoback 1992). References: 1 – Lazareva and Misharina (1965), 2 – Savostin and Karasik (1981), 3 – Bungum and Fyen (1979), 4 – Bungum and Kristoffersen (1980), 5 – Bungum et al. (1979), 6 – Vaage (1980), 7 – Kibsgaard (1985), 8 – Mitchell et al. (1990), 9 – Chan and Mitchell (1985), 10 – Havskov and Bungum (1987), 11 – Hansen et al. (1989), 12 – Lindholm and Havskov (1989), 13 – Bungum et al. (1991), 14 – Bungum & Lindholm (1996), 15 – Engell-Sørensen (pers. comm. 1994), 16 – Lindholm et al. (1995), 17 – Fejerskov et al. (1996), 18 – Hicks (1996), 19 – Atakan et al. (1994), 20 – Inst. of Solid Earth Phys., Univ. of Bergen, 21 – Hicks et al. (2000), 22 – this paper.

similar distances (three stations at 20–40 km), so the modelling results are comparable in quality to those from the 99.04.09 earthquake. The third earthquake where waveform modelling has been used is 99.09.02, which however occurred at a greater distance from the available stations. With five stations up to 114 km distance the modelling in that case has been used mostly in terms of phase (P/S) amplitude ratios, which for those distances are more robust than the full waveforms in constraining the solution. Still, this solution has a lower quality rating. The remaining four new solutions have been determined from first-motion data alone, all reasonably well constrained.

Two of the new solutions are located close to the coast in mid-Norway (99.04.09 and 99.08.23). They both show a normal fault movement, have an approximately E–W orientation, shallow plunging T axis. The other five solutions are from western Norway, the solution from the 99.08.02 earthquake is located in the northern North Sea inversion box, the other four fall into the Onshore West Norway box. The five solutions comprise one normal fault, two reverse and one strike-slip and one oblique reverse/strike-slip.

Database

The list of 112 earthquake focal mechanism solutions is compiled from a number of published sources and updated with the seven new solutions discussed above (Table 1). Solutions outside the inversion regions are also included, mainly comprising seven solutions in the oceanic crust of the Norwegian Sea and the Mohns ridge, and six solutions in and around Svalbard. The date, location, depth and magnitude are given (composite solutions are assigned magnitudes of − 1.0), while the focal mechanism

solution is given by trend (trn) and plunge (plg) of the T (tension) and P (compression) axes. The direction of maximum horizontal compressive stress (σ_H) is calculated according to Slunga (1981), quality (Qual.) and stress regime (Reg.) are according to criteria defined in the World Stress Map project (e.g. Zoback 1992). The maximum horizontal compressive stress directions from all available stress data (earthquake focal mechanism solutions and in situ data) are plotted in Fig. 3, with colour code differentiating on stress regime. In Fig. 3 we have also indicated the eight zones (boxes) within which we have been inverting for a common (dominating) stress region, where the ones furthest south (southern North Sea) and north (western Barents Sea) contain only in situ data (borehole breakouts). Note that there is an overlap of the Northern North Sea and Offshore Mid-Norway zones between 62 and 63° N. The reason for this is that these events are transitional and therefore tectonically could belong to both zones; also, this will increase the number of solutions in each zone and thereby improve the accuracy of the inversions, which applies ·in particular to the Offshore Mid-Norway zone.
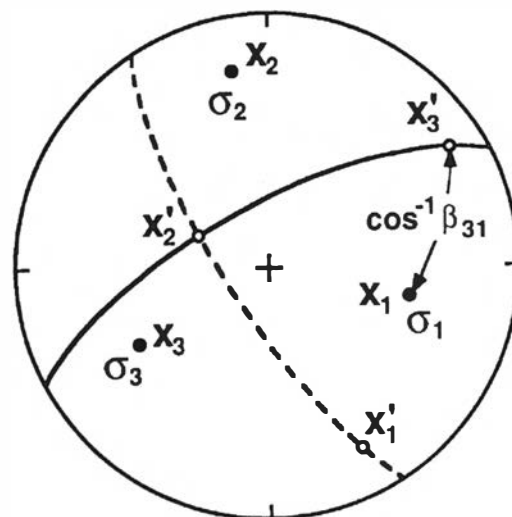

Fig. 4. The two Cartesian coordinate systems used in the FMSI inversion, where x_i are principal stress axes. Fault geometry axes (x_i') are fault pole, B axis and slip direction. Solid great circle is fault plane, dashed is auxiliary plane. Transformation matrix $\beta_{ij} = \cos(x'_i \wedge x_j)$. After Gephart (1990a).

Stress inversion of focal mechanism solutions

Principles of analysis

The P and T axes defining a focal mechanism solution, located 45° to the two nodal planes, represent the orientation stress axes that result in the highest shear stress on these planes. However, rupture in competent rock generally occurs at an angle closer to 30° to the primary principal stress axis according to the Mohr–Coulomb failure criterion, so there is an approximately 15° discrepancy between the P and T axes and the axis of principal stress. In addition, rupture on pre-existing faults and zones of weakness can occur at an even wider range of angles with regard to σ_1, thus introducing a large uncertainty in the principle stress orientation one can imply from single focal mechanism solutions. Inversion is one method of reducing this uncertainty, by considering groups of focal mechanisms assumed to derive from a common stress tensor.

Stress inversion of the available focal mechanisms was done using the FMSI (Focal Mechanism Stress Inversion) package by John Gephart (Gephart 1990a), based on procedures described by Gephart & Forsyth (1984) and Gephart (1990b). The principle involved defines the misfit of a given mechanism with regard to a stress model as the minimum rotation required to bring each nodal plane into compliance with the stress model being tested (Fig. 4). Unless one plane has been uniquely identified as the actual fault plane, the plane with the smallest rotation angle is considered to be the fault plane. The programme also assesses the magnitude of the intermediate principal stress axis σ_2 in relation to σ_1 and σ_3, looping over a set interval for this relation, denoted R. The nodal plane for each input

solution best corresponding with a given model is thus selected. This procedure allows for errors both in fault plane orientation and slip direction. For each stress model tested, the rotation magnitudes are summed for all data, resulting in a single measure of misfit for each model, where the models with the lowest misfit value have the best fit to the combined data for that inversion. The stress models and corresponding misfit values are determined through a simple grid search, which is a reliable, albeit computation intensive, approach to achieve convergence for non-linear problems.

Method of analysis

The available earthquake focal mechanism solutions were separated within the inversion boxes shown in Fig. 3, and the P and T axes checked for orthogonality as a quality check against possible data input or conversion errors. As the solutions have quality designations from A (best) to D (worst) according to the World Stress Map (e.g. Zoback 1992), their contribution to the inversion was weighted 2.0 (A), 1.66 (B), 1.33 (C) and 1.0 (D). The inversion was performed on the solutions from each zone using FMSI (Gephart 1990a), calculating the misfit value for a total of over 300,000 stress models with covering the entire hemisphere at a 5° interval, with the R value for varying from zero ($\sigma_2 = \sigma_1$) to one ($\sigma_2 = \sigma_3$). In addition, eight (of 34) strongly rotated solutions in the Northern North Sea were separated from the remaining solutions in this zone, and separate inversions performed on these two groups.

Confidence limits were calculated based on the misfit values using the method defined in Gephart & Forsyth (1984), based on one-norm misfit statistics (Parker & McNutt 1980). The confidence intervals for 95%, 68% and 10% for σ_1, σ_3 and R for each zone are shown in Fig. 8.

Table 2. Overview of stress generating mechanisms (after Fejerskov & Lindholm 2000).

Stress field	Lateral endurance	Stress generating mechanisms
1st order Continental	>1000 km	Plate tectonic forces • Ridge push • Basal drag • Slab pull
2nd order Regional	100–1000 km	Large-scale density inhomogeneities • Continent-ocean boundary Flexural stresses • Sediment loading • Deglaciation Wide topographic loads
3rd order Local	<100 km	Topography • Fjords • Mountain ranges Geological features • Faults • Hard and soft inclusions

Crustal stresses inferred from earthquake data

The crustal stresses for each of the eight regions are discussed based on available data. The regions have been selected based on data availability, seismic activity and crustal regime, and are of sufficient size that the first and second-order stresses (continental and regional scale, cf. Table 2) should be reflected in the inversion results, while the third-order (local) stresses should be reduced as they are of a more random nature. Table 2 lists some stress generating mechanisms for the different scale stresses (Fejerskov & Lindholm 2000; see also Byrkjeland et al. 2000).

For each of the six zones containing earthquake focal mechanism solutions (zones a–f), the individual observa-tions are shown in three different ways. In Fig. 5 the individual P and T axes are plotted stereographically with different symbols, in Fig. 6 the directions of the maximum horizontal compressive stress (σ_H) are shown in terms of rose diagrams, properly weighted with respect to quality, and in Fig. 7 the actual focal mechanisms are shown on tripartite plots where the three principal modes of faulting are connected to different corners in the triangles using the technique of Frolich and Apperson (1992). The last type of presentation is particularly useful in that the degree of obliqueness is so well facilitated.

The results of the inversions for each of the six zones (a–f) are shown in Fig. 8, including the separate inversions of the two groups of focal mechanism solutions (rotated and non-rotated) in the Northern North Sea zone, plotted stereographically, and with indications of the resolution in each particular case. In general it is seen that while the individual solutions are quite scattered, they are still complying reasonable well with one common stress field orientation. What this first of all demonstrates is that the focal mechanism is reflecting the interaction between a regional stress field and the local conditions where the earthquake occurs, primarily existing zones of weakness.

The R-values lie in the 0.3 to 0.7 range for all zones, meaning than the magnitude of the intermediate principal stress (σ_2) is fairly close to midway between the magnitude of the σ_1 and σ_3 axis (R = 0.5).

For each of the six zones, supplemented by the western Barents Sea (zone g) and the southern North Sea (zone h), we also show available insitu stress measurements. Finally, in Fig. 10, we present a summary of the inversion results, directly based on Fig. 8, along with the two extra in situ zones. We now proceed to a discussion of each of the six zones in more detail.
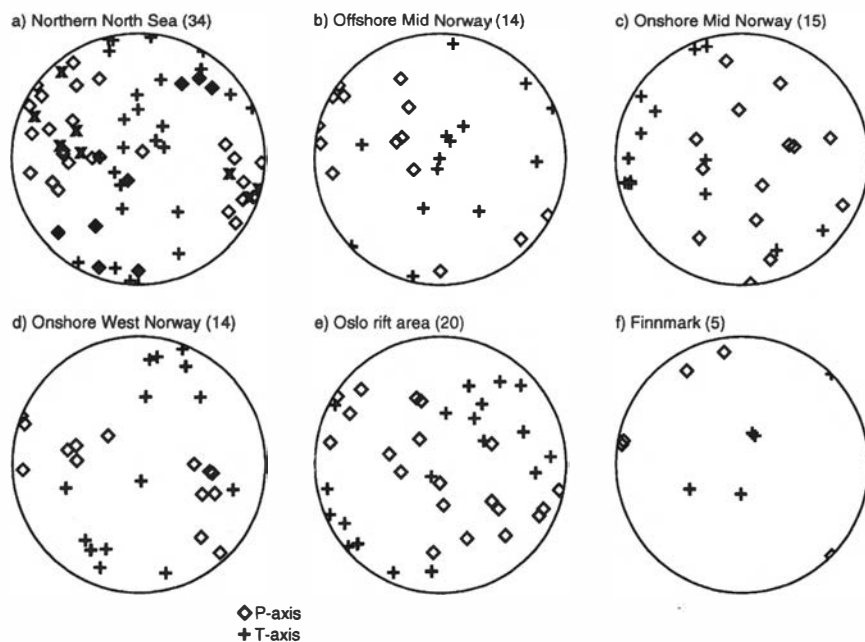

Fig. 5. Stereographic plots of P (compression) and T (tension) axes from all the earthquakes within each inversion area (defined in Fig. 1), shown as diamonds and crosses, respectively. The number of solutions in each area is given in parenthesis. The eight rotated (more than ~60° compared to the nonrotated trend) solutions within the northern North Sea area are shown as filled diamonds and oblique crosses for the P-and T axes. The rotation of these mechanisms with regard to the other solutions in this area is apparent, and separate FMSI inversions on the two groups of data have also been performed.
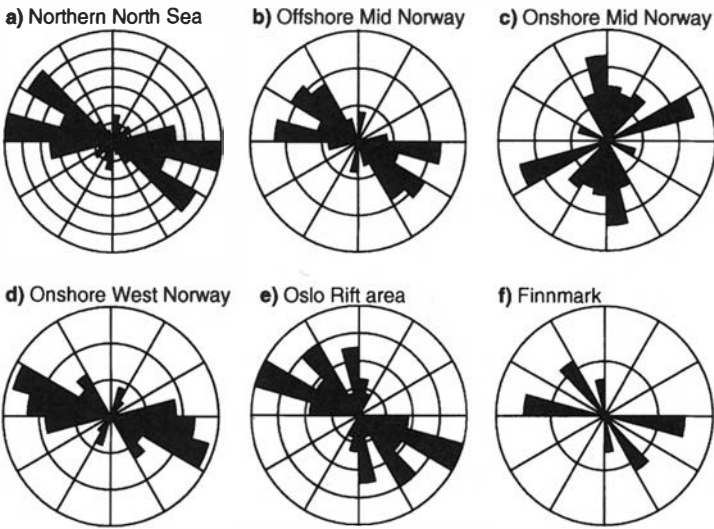
Fig. 6. Directions of maximum horizontal compressive stress as derived from the earthquake focal mechanism solutions for each inversion area (defined in Fig. 1). Each concentric circle represents one WSM 'A' quality solution (weight 2.0) or two 'D' quality solutions (weight 1.0). 'B' and 'C' quality solutions have weights of 1.66 and 1.33, respectively.

Northern North Sea (zone a)

The northern part of the North Sea is one of the most seismically active areas in Norway, and a large number of earthquake focal mechanism solutions exist for this zone (34). As can be seen in Fig. 5a, there is a quite large scatter in the distribution of the P and T axes overall, although two trends are visible in that the majority of the solutions (26) have a WNW–ESE direction for the P axes, while the remaining eight solutions exhibit an almost 90° rotation of the P and T axes. These eight solutions are shown by filled diamonds and diagonal crosses. This WNW-ESE trend is also visible in the rose diagram (Fig. 6a) for the maximum horizontal compressive stress (σ_H) directions as derived from the individual earthquake focal mechanism solutions. The faulting mechanisms in this zone (Fig. 7a) seem to be

organized in two groups; reverse to oblique-reverse and normal to strike-slip, although there is no apparent systematic distinction between the eight rotated focal mechanism solutions and the remaining 26 solutions. There are also no systematic differences in depth or location between these two types of mechanisms in this area.

The inversion results for all data in this zone (Fig. 8a) show a σ_1 axis with a fairly shallow plunge, and a trend close to E–W (see also Table 3), which should be considered a composite of the two distinct trends visible in Fig. 5a. The confidence limits cover a fairly large area due to this large scatter in the input data. However, the separate inversion results for the rotated and nonrotated solutions show a clearer picture. The 26 nonrotated solutions have very well defined σ_1 and σ_3 axes with a
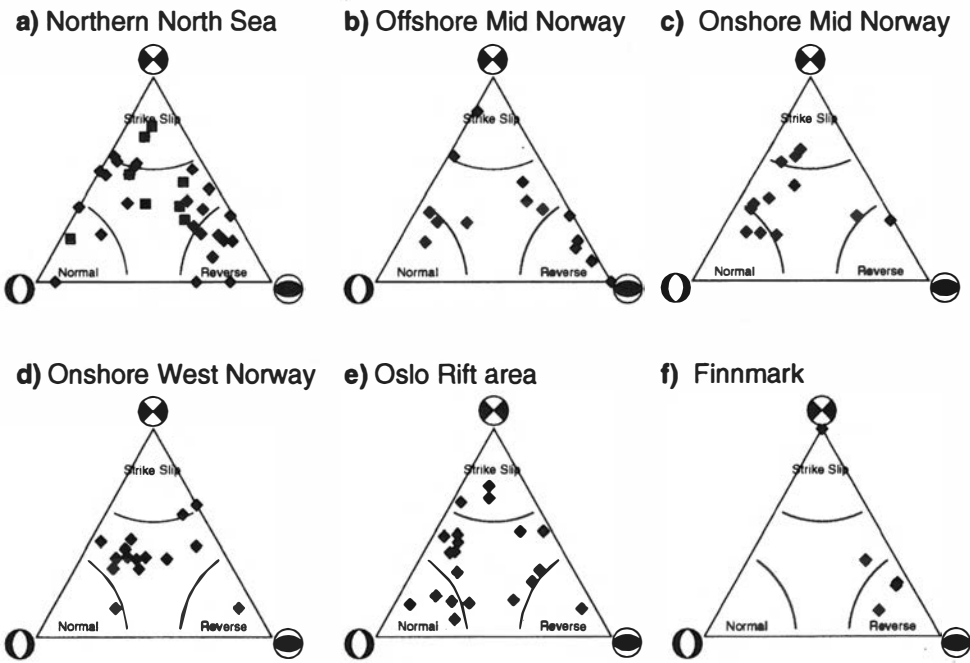

Fig. 7. Triangle plots (Frolich and Apperson 1992) of fault regime distribution of the earthquake focal mechanism solutions for the six areas. The corners represent mechanisms where the B axis is oriented vertically (pure strike-slip) or horizontal (pure normal/reverse). The arcs represent a 30° deviation of the B axis from the perfect case, defining within each triangle the area that for practical purposes could be considered to contain "pure" solutions. The solutions located elsewhere, i.e., within the central parts of the triangles, would thereby be considered to represent oblique faulting. The eight rotated solutions in the Northern North Sea are plotted as squares, showing no distinguishing trend compared to the other solutions.
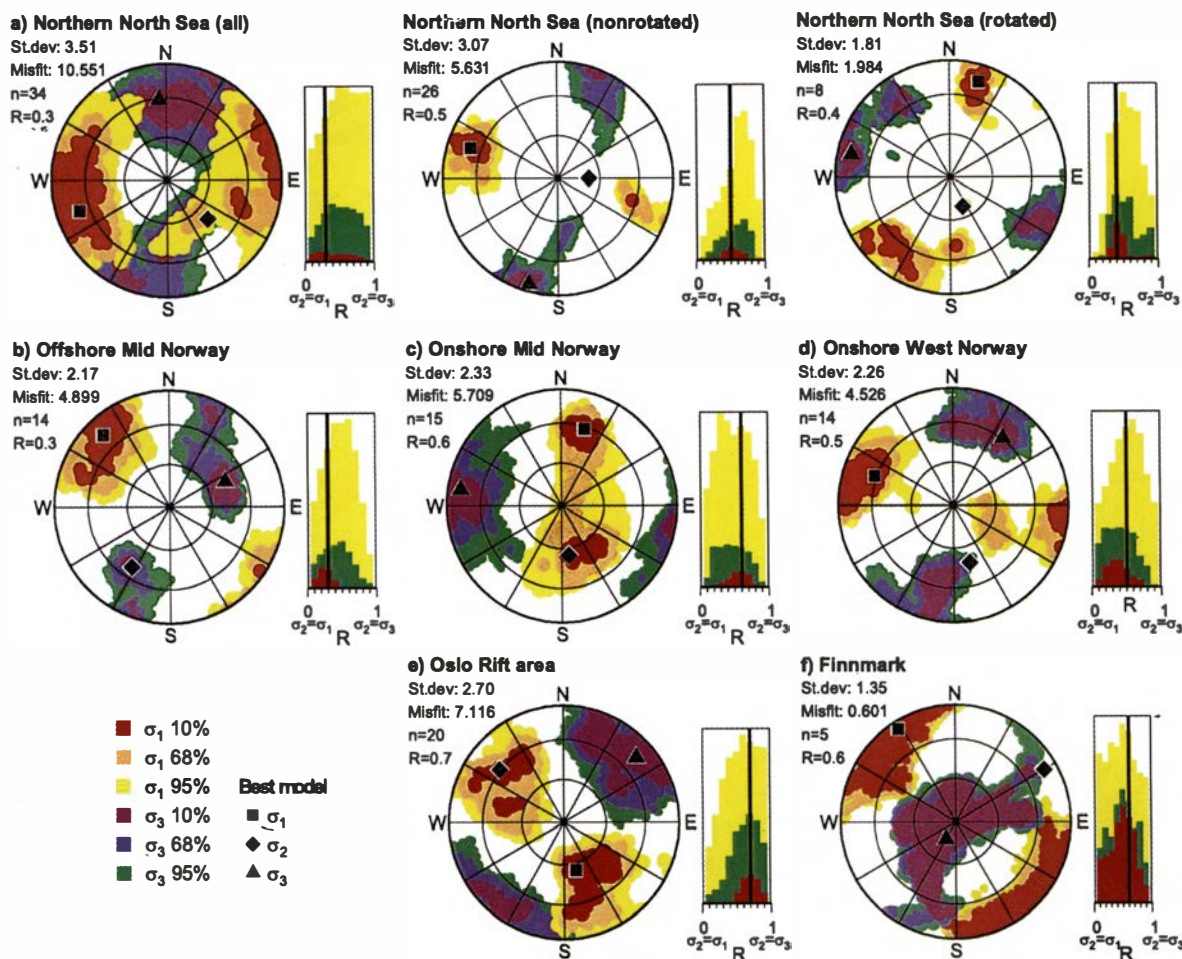
Fig. 8. Results by confidence from the inversion of the earthquake focal mechanism solutions, plotted stereographically. The best stress model is shown for each zone. The result from the inversion of eight rotated solutions in the northern North Sea zone shown separately (top right), as are the 26 remaining solutions in this area (top middle). The inversion results of all 34 solutions in this zone are also shown. Note the unstable results of the inversion of the data from Finnmark, due to the low number of data points available. The yellow, green and red areas in the R-value histograms represent the 95%, 68% and 10% confidence limits, respectively.

shallow dip and a WNW–ESE compression, corresponding well to the main trend of individual σ_H directions visible in Fig. 6a. The eight rotated solutions have also have similarly well-defined σ_1 and σ_3 axes with shallow dips, but rotated almost exactly 90° compared to the results based on the nonrotated solutions.

The in situ σ_H data from borehole breakouts shown in Fig. 9a are more scattered, however, but a weak trend in the E–W to NW–SE direction is visible.

The WNW–ESE direction of maximum compressive stress derived from the 26 non-rotated focal mechanism solutions in this zone is compatible with the expected direction of the ridge-push force in this zone (Bungum et al. 1991). The NNW–SSE direction defined by the eight rotated solutions imply some other, more local, source of crustal stress in this area, either a NNW–ESE horizontal compression or a WNW–ESE horizontal tension that is locally sufficiently strong to cause an interchange of the σ_1 and σ_3 axes. The similarity of the eight rotated solutions, which are scattered over the entire Sogn Graben area, could imply a common source, however, the fact that there

are a number of nonrotated solutions in the same area gives rise to the question why only a few of the earthquakes have inverted σ_1 and σ_3 axes.

Offshore Mid-Norway (zone b)

As can be seen from Fig. 1, the mid-Norwegian margin has a band of relatively high seismic activity running roughly parallel to the shelf edge through the East Vøring Basin, where evidence suggests that the prominent Plio-Pleistocene glacial wedge may be one of the main factors influencing the stress field responsible for this activity (Byrkjeland et al. 2000). The offshore activity here is separated from the coastal activity by the more or less aseismic Vøring Shelf (Trøndelag Platform). The depth estimates for these earthquakes are uncertain due to the large hypocentral distances, but available evidence, based in part on waveform modelling (NORSAR and NGI 1998) suggests that most of the earthquakes occur deeper than 15 km. There are 14 available earthquake focal mechanism solutions in this zone. The trend of the P axes shown in Fig.

Table 3. Earthquake focal mechanism stress inversion results for the six areas.

Area	No. of F.M.s	FMSI misfit	σ	R	σ_1 trn	σ_1 plg	σ_2 trn	σ_2 pln	σ_3 trn	σ_3 pln
(a) Northern North Sea (all)	34	10.551	3.51	0.3	251	21	133	50	355	31
Northern North Sea (nonrot.)	26	5.631	3.07	0.5	289	21	90	68	196	7
Northern North Sea (rot.)	8	1.984	1.81	0.4	17	17	157	68	283	13
(b) Offshore Mid-Norway	14	4.899	2.17	0.3	317	17	213	39	66	46
(c) Onshore Mid-Norway	15	5.709	2.33	0.6	17	32	172	55	279	12
(d) Onshore West Norway	15	4.526	2.26	0.5	290	28	164	48	37	29
(e) Oslo Rift area	20	7.116	2.70	0.7	166	55	309	29	49	17
(f) Finnmark	5	0.601	1.35	0.6	328	7	60	12	210	76

For each geographical area (Figs. 1 and 9) the table gives number of focal mechanisms, relative misfit number (see main text), and trend and plunge of the three orthogonal stress axes of the stress tensor.

5b is quite consistent, as all but one of the focal mechanism solutions lie in a NW–SE trending band, and this solution is in the boundary area to the more complex northern North Sea (zone a). This is also seen in the rose diagram in Fig. 6b, with all the σ_H directions but one being confined to a 60° segment with a E–W to NW–SE trend. Fig. 7b shows that the modes of faulting in this zone are organized more or less in the same way as further south in the Northern North Sea, with a balance between reverse and normal.

The FMSI inversion (Fig. 8b) shows a best fitting stress tensor with a shallow plunging σ_1 axis in the NW direction. The confidence limits indicate a fairly stable inversion where the σ_1 axis appears to be well constrained, while the σ_2 and σ_3 axes are more ambiguous, as the σ_2 axis is located within an alternative likely σ_3 orientation. There are fewer in situ measurements in this zone (Fig. 9b), but

they also have a quite clear NW–SE trend. It would appear that the offshore areas of mid-Norway have a fairly stable stress field, given the consistency of the data in this zone, also between different data types. While the direction of maximum horizontal compressive stress is compatible with the expected direction of the ridge-push force in this area also, it also happens to be perpendicular to the orientation of the glacial wedge and to the continental margin itself, with significant lateral crustal inhomogeneities (cf. Byrkjeland et al. 2000).

Onshore Mid-Norway (zone c)

The onshore parts of mid-Norway have a noticeable pattern of seismic activity in that the southern parts are almost completely aseismic while the northern parts have
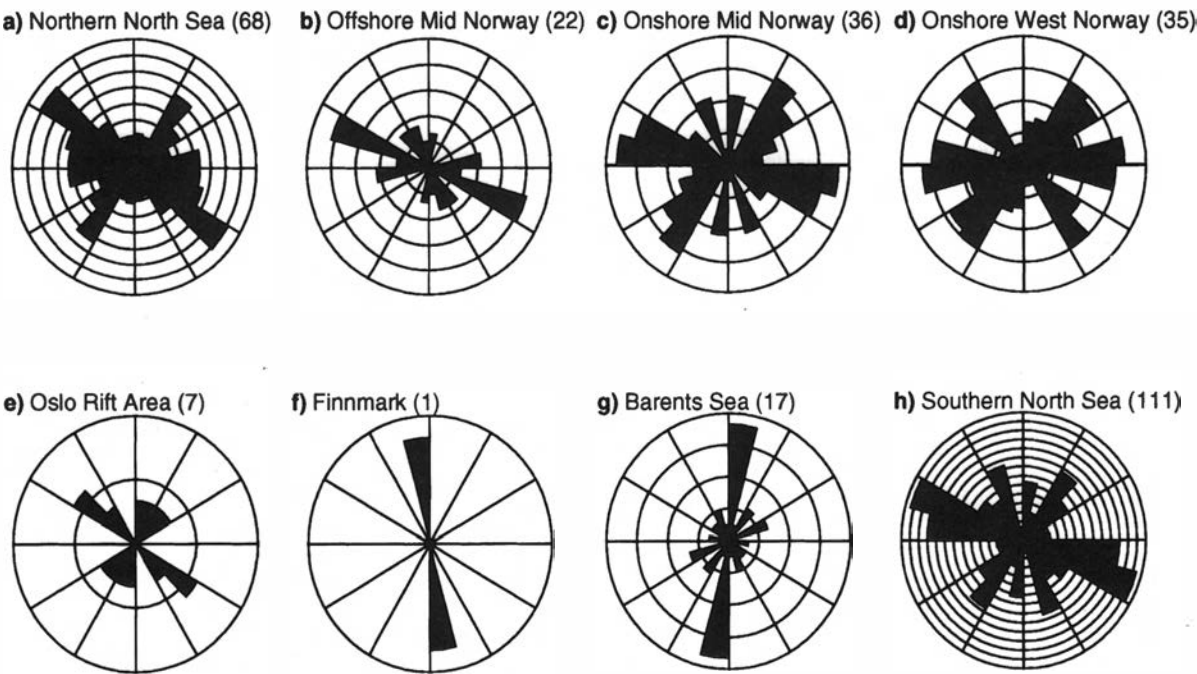

Fig. 9. Directions of maximum horizontal compressive stress from in situ measurements for each of the six earthquake inversion areas, in addition to data from the western Barents Sea and the southern parts of the North Sea. The measurements consist of borehole breakouts offshore and overcoring measurements onshore. The weighting is the same as for Fig. 6.

significantly higher levels of seismic activity, having experienced several shallow (depth less than 12 km) earthquake swarms in recent years (Bungum et al. 1979; Atakan et al. 1994; Hicks et al. 2000). The largest onshore earthquake known from historical times in Norway, the 31 August 1819 Rana earthquake with a magnitude of M_S 5.86.2 (Muir Wood 1989), also occurred in this area.

The P and T axes for the 15 available earthquake focal mechanism solutions in this zone are quite scattered (Fig. 5c), although there does appear to be a weak trend for the P axes to have azimuths in an approximately N–S band. Similarly, the tension axes have a weak tendency towards a NW–SE orientation. This is the exact opposite of the offshore areas to the west (Fig. 5b). This trend is not readily apparent in the σ_H rose diagram (Fig. 6c), but this is due to the single WSW–ENE bin containing three solutions. The five bins from NNW–SSE to NE–SW contain a total of 11 solutions, so there is a very real trend of compressional stress centred around a N–S orientation visible in the earthquake focal mechanism solution data. Fig. 7c shows that the faulting is predominantly in the normal to strike-slip range, as reflected also in the noted differences in T axis orientations.

The FMSI inversion results (Fig. 8c) show a similar picture to the individual solutions, with the σ_3 axis having a shallow plunge in a WNW direction. In contrast to the nearby offshore areas, the σ_3 axis is the one best constrained by the inversion results, while the σ_1 and σ_2 axes appear to be more interchangeable. This implies that a WNW–ESE tension is the controlling stress factor in this area, which is nearly the exact opposite to the offshore areas to the west, and also with respect to the expected direction of the ridge push force from the Mohns ridge in the North Atlantic. Recent compilations of postglacial uplift data (Dehls & Olesen 1999; Hicks et al. 2000) indicate that the contemporary uplift in this area is not necessarily as uniform as previously thought to be the case. The onshore seismic activity in mid-Norway occurs within the areas that have the highest uplift gradient, which could be considered a bending force in the crust. This force could be a source of shallow, coast-normal extension, and is thus a likely candidate for explaining the shallow seismic activity and inverted stress field observed in this area (Hicks et al. 2000). The difference in seismic activity from south (low) to north (high) may have a connection to topographic effects; the areas south of ~66°N are comparatively flat and of low elevation, while the region further north has a much more pronounced topographic relief, with large regions of high elevation.

The in situ data (Fig. 9c), which consists of overcoring measurements mainly taken in or near mines are more scattered. There appears to be two trends, one sub-parallel to the coast (NE–SW) and the other roughly normal to the coast (WNW–ESE), but there does not appear to be any systematic distribution of the two main σ_H trends with location. If the rotation just seen in the earthquake P axis directions was due to a systematic regional crustal source of stress we should have expected to see a σ_H rotation also

in the in situ data in the seismically active northern areas, but this does not appear to be the case. However, one would always expect more scatter in situ data, and from overcoring measurements in particular, in particular the shallow measurements are influenced by local effects (Table 2) to a much higher degree than the earthquake focal mechanism solutions.

Onshore West Norway (zone d)

The onshore western Norway zone is located in close proximity to the areas of relatively high seismicity in the northern North Sea, revealing a similarly high seismic activity (Fig. 1). The 15 earthquake focal mechanism solutions available in this zone appear to be quite consistent in terms of P and T axis distribution (Fig. 5d), with the P axes aligning in an WNW–ESE direction and with the T axes oriented at 90°. This is reflected by the σ_H directions in the rose diagram in Fig. 6d, and with a consistency which is quite striking. Almost all of the available focal mechanism solutions here are oblique (Fig. 7d), but clustered in the normal to strike-slip region.

The stress inversion results do not contradict this, as the σ_1 axis is quite well constrained, with an WNW direction and shallow plunge (Fig. 8d). This is almost identical to the inversion results based on the nonrotated focal mechanism solutions in the northern North Sea zone to the west. The σ_2 and σ_3 axes are somewhat more uncertain, the best model gives the σ_3 axis a fairly shallow plunge to the NE, but the confidence limits define a much larger area varying up to 90° in plunge, but in general in a NE–SW direction. This is most likely a result of a slightly different dominant faulting regime onshore, where the focal mechanism solutions tend slightly toward normal faulting, while strike-slip and reverse faulting is more predominant offshore. There is a quite distinct hypocenter depth difference as well, with the onshore earthquakes generally having shallower hypocentral depths (<15 km) as compared to the greater depths (>15 km) encountered offshore.

The in situ data, consisting of overcoring measurements, appear to have a near random distribution, again implying that the shallow measurements are strongly influenced by local (third-order) stress generating mechanisms (Table 2).

Oslo Rift area (zone e)

The Permian Oslo rift has intermediate levels of seismic activity, somewhat higher than the surrounding basement areas. Due to the location of the NORSAR seismic array in this area, the number of available earthquake focal mechanism solutions is quite high (20), while the magnitudes for the solutions are generally somewhat lower.

The hypocenter depths range through the entire crust, from shallow (<5 km) to more than 30 km. The P and T axes for the individual focal mechanism solutions appear to be quite systematic (Fig. 5e), with the P axes aligned in a NW–SE trending band. The rose diagram of the focal
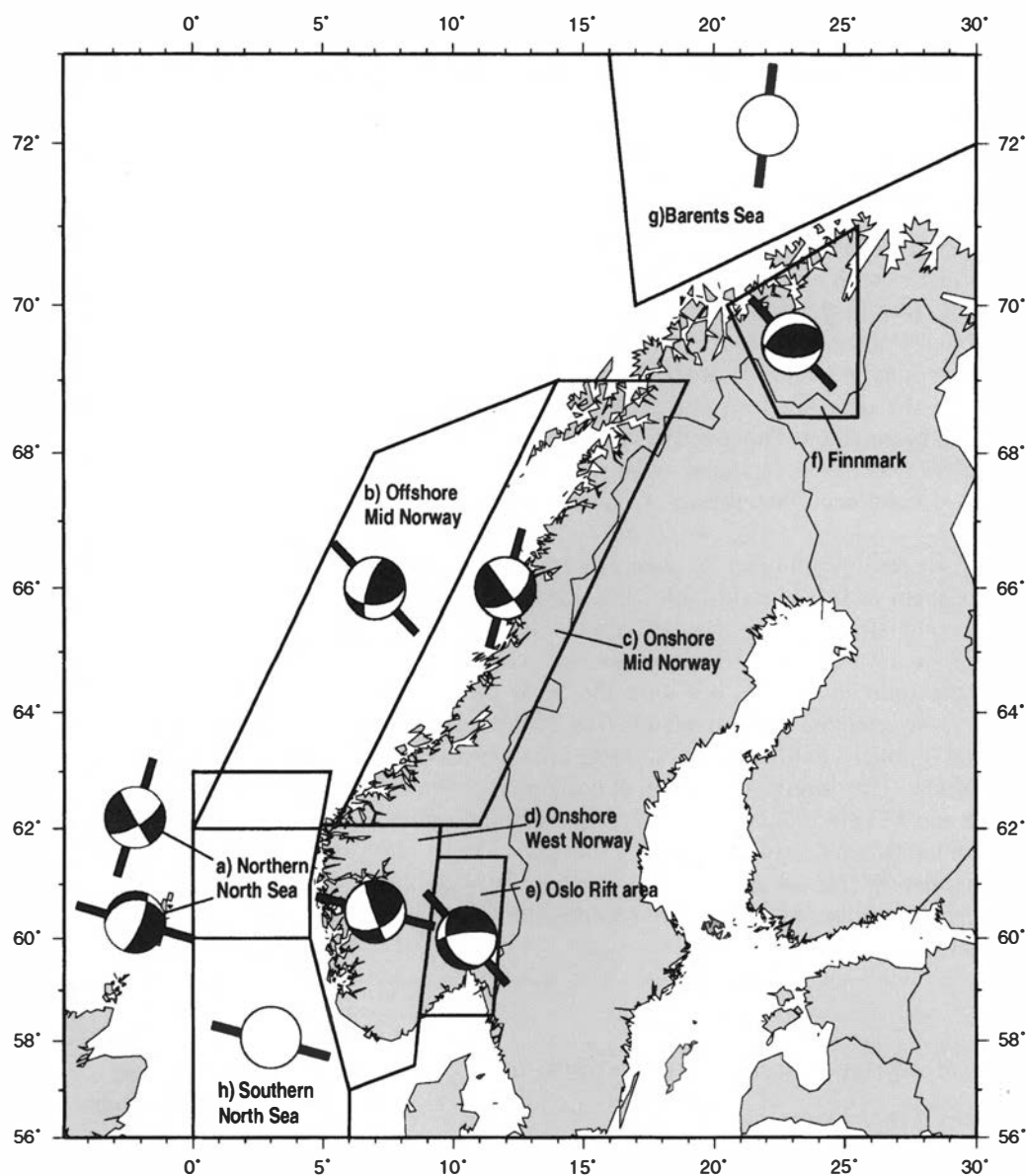
Fig. 10. Composite focal mechanism solutions derived from the inversion results for each area. Both inversions of solutions from the northern North Sea data (rotated and nonrotated) are shown, reflecting the bimodality observed in this area. The western Barents Sea and southern North Sea areas are plotted as open circles, as the only available data there are borehole breakouts with σ_H values only.

mechanism σ_H directions (Fig. 6e) also shows a similar trend, although somewhat more scattered than for the data from western Norway. The faulting mechanisms here (Fig. 7e) seem to be organized mostly as for onshore mid-Norway, mostly normal to strike-slip, but some also towards the reverse side. There does, however, appear to be some variation of faulting regime with depth in the Oslo Rift zone, with the shallow (<13 km) earthquakes being of predominantly normal faulting while the deeper earth-quakes are dominated by strike-slip and reverse faulting (Hicks 1996).

The FMSI inversion gives a best fitting stress model with a poorly constrained, steeply plunging σ_1 axis (50°), trending towards the SSE (Fig. 8e; Table 3). The σ_2 axis of the best model is located within another area where the confidence limits imply a possible σ_1 location, implying that the inversion algorithm was not able to differentiate the σ_1 and σ_2 axes with any significant accuracy. The σ_3 direction appears to have a quite large uncertainty, with an

approximate NE–SW direction. The direction of horizontal compression is quite similar to the onshore West Norway zone to the west, but the plunge of both the possible σ_1 axes is much steeper. This is a significant rotation compared to the adjacent zone in western Norway, probably related to a second-order stress generating mechanism, possibly the rift structure itself. Only seven in situ measurements are available for this zone, so no significant information can be inferred from this. However, based on the generally large scatter in overcoring measure-ments in western and mid-Norway, it does not appear as if overcoring measurements can offer much meaningful data on regional or continental scale stresses in any case.

Finnmark (zone f)

Finnmarksvidda is an area that is, in general, considered to have low levels of seismic activity. A relatively large earthquake occurred in 1996, with a magnitude of M_L 4.0,

the largest in this region in 60 years (Bungum & Lindholm 1996; Hicks 1996). This earthquake, and five others with magnitudes ranging from M_L 1.4 to 3.3 all have shallow hypocenter locations within 10 km southeast of a large, postglacial fault striking NE–SW (Olesen 1988; Bungum & Lindholm 1996).

With only five focal mechanism solutions available in this zone, one cannot normally expect to be able to infer a stress model with any significant certainty; however, it is apparent from Fig. 5f that all five solutions have near-horizontal P axes in an approximately NW–SE direction. The rose diagram (Fig. 6f) of the σ_H directions is similar, although the data are too scarce for any more detailed trends to be apparent. The mechanisms (Fig. 7f) are almost all purely reverse in this case, fully consistent with the strong neotectonic observations from this area (Olesen 1988).

Due to the low number of data points, the inversion results seem to be quite unstable (Fig. 8f; Table 3). The best fitting stress model has an almost horizontal σ_1 orientation in a NW–SE direction, as one would expect from the individual data, but with the 95% confidence interval covering the entire quadrant. The 95% confidence interval for the σ_3 axis also covers a large area surrounding the vertical. The observed direction of horizontal compression is most likely influenced by the major weakness zone in Finnmark, but still implies a tectonic force in approximately the same direction, compatible with the expected direction of horizontal compression from the mid-Atlantic spreading ridge.

Crustal stresses inferred from in situ data

Western Barents Sea (zone g)

The western Barents Sea has very low levels of seismic activity, which combined with the fact that the distance to any seismic stations is large means that there are no earthquake focal mechanism solutions available. However, the 17 available borehole breakouts are surprisingly consistent in σ_H directions (Fig. 9g), with nearly 2/3 of the data lying within the same 15° bin with a NS trend. The boreholes are scattered over a large area in the southern parts of the western Barents Sea, so it would appear that this is a real trend.

Southern North Sea (zone h)

The southern parts of the North Sea have, in contrast to the regions to the north, low to intermediate levels of seismic activity. This means that there are currently no earthquake focal mechanism solutions available. However, due to extensive hydrocarbon exploration in this area, a large number of borehole breakouts are available (111). Although the σ_H directions are quite scattered, there is a fairly consistent trend visible in the WNW–ESE direction (Fig. 9h). The low seismic activity of this area suggests that

there are no dominant stress generating mechanisms active in this area capable of inducing the differential stresses required for higher levels of seismic activity, but the in situ data suggest that there is a compressive force in the WNW–ESE direction, quite possible originating from the mid-Atlantic ridge.

These results from the southern North Sea are in a clear contrast to similar in situ results reported from further south in the Central Graben (Ask 1998), where the stress data are much more scattered, essentially random. The difference here is expected somehow to be related to a difference in the ability of the sedimentary rocks in the two regions to support regional stress propagation (Bjørlykke 1995; Bjørlykke & Høeg 1997).

Concluding remarks

The results as obtained through the earthquake stress inversions for the six regions in southern, central and northern Norway are summarized in Table 4 and Fig. 10, complemented by two regions (southern North Sea and western Barents Sea) from where only in situ stress measurements are available. The regional differentiation in terms of modes of faulting as shown in Fig. 7 reflects a considerable scatter but at the same time interesting systematic differences, and the main observation here is a tendency (albeit weak) for reverse to strike-slip faulting in offshore areas (a–b) and normal to strike-slip in onshore areas (c–e), as discussed in more detail elsewhere (e.g. Stein et al. 1979; Byrkjeland et al. 2000). The quality and resolution of these observations are, however, considerably improved in the present study as compared to what has been documented earlier.

The inversion results basically show stress directions which comply quite well with the directions expected from the plate-wide first-order gravitational force from the mid-Atlantic spreading ridge (Fejerskov & Lindholm 2000). This is the so-called ridge push, which by definition should be perpendicular to the spreading ridge (and not necessarily following the flow lines for the spreading, which is often assumed). The different direction in the western Barents Sea is not necessarily an exception here since the ridge push force there should be expected to be different both in direction and strength, reflecting the change both in direction, morphology and rheology as one moves from the Mohns Ridge and into the Knipovich Ridge.

This coincidence between observed and predicted stress directions, as seen clearly also globally (Zoback et al. 1992), is a strong indication of an acceptable physical mechanism, but it is not sufficient for unequivocally concluding that what we see is a ridge push domination within all sub-regions in our study. The reason for this is that for some of these sub-regions we have second-order sources of stress (cf. Table 2) which should be expected to be oriented in the same direction, first of all large-scale density inhomogeneities across the continental margin and

Table 4. Summary of the eight areas within which stress inversions are performed.

Area	Tectonic regime	Seismic activity level	Focal depths	Modes of faulting	σH direction
Northern North Sea	Triassic–Cretaceous rifted margin	Very high	Deep	Reverse to oblique-reverse Normal to strike-slip	NW–SE (also NNE–SSW)
Offshore Mid-Norway	Cretaceous–Paleocene volcanic rifted margin	High	Deep	Reverse to oblique-reverse Normal to strike-slip	NW–SE
Onshore Mid-Norway	Caledonian thrust belts	High in northern parts. Earthquake swarms	Shallow	Normal to strike-slip	NNE–SSW
Onshore West Norway	Precambrian shield, thrust belts to the north	High	Shallow	Oblique at the normal to strike-slip side	ESE–WNW
Oslo Rift Zone	Permian rift	Intermediate	All	Normal (shallow) Reverse to s-s (deeper)	E–W
Finnmark	Precambrian basement, thrust belts near coast	Low	Shallow	Reverse	NW–SE
Western Barents Sea	Jurassic–Tertiary rift with later uplift	Very low			N–S
Southern North Sea	Triassic–Cretaceous rifted margin	Low	Deep	Unknown	ESE–WNW

The seismic activity levels used in the table are relative for Fennoscandia. Focal depths are denoted 'deep' when the bulk of earthquakes occur below 15 km, and 'shallow' when most of the earthquakes have depths less than 15 km. Similar principles are applied for stress regimes and stress directions.

farther into the Fennoscandian shield. Even more locally, third-order sources of stress are expected to come into play. In an extensive review of this problem Byrkjeland et al. (2000) have concluded, from a combined study of seismicity distribution, inferred stress and stress model-ling, that such higher order sources of stress are in fact needed in order to explain the seismicity in our study region. Another support for a reflection of more local effects in our focal mechanisms is the difference in mode of faulting between onshore and offshore areas, showing a tendency for normal (and also more shallow) faulting onshore and strike-slip and reverse faulting offshore, as also expected theoretically (Stein et al. 1979).

One of the interesting observations in the available focal mechanism database presented here is the 90° rotation of σ_H for a number of focal mechanism solutions in the Sogn Graben/ Tampen Spur area and in the coastal parts of Nordland (Rana), demonstrating significant local stress variations as well as the importance of local stress sources. Such a rotation was noted for the first time by Bungum et al. (1991) and has been discussed often since then (Lind-holm et al. 1995; 2000; Hicks et al. 2000; Byrkjeland et al. 2000), but explained generally only as an interchange of σ_H and σ_h (the largest and smallest horizontal stress compo-nents) which more easily can been achieved when the σ_H/σ_h ratio is not far from unity. This would most easily be feasible in thrust-faulting regimes where σ_3 is vertical and in normal-faulting regimes when σ_1 is vertical, allowing σ_H and σ_h to be close to each other. An example here is an in situ measurement from 100 m depth in Bidjovarre, Finn-mark (Dehls & Olesen 1999), where σ_1 and σ_2 both were of the order of 15–17 MPa and σ_3 was 12–13 MPa.

It has already been noted that a likely explanation for the rotation observed in the Nordland area is postglacial uplift, as the uplift gradient is highest in the coastal area, implying shallow earthquakes with coast-normal extension (Hicks et al. 2000). Such mechanisms are consistently seen in that region. In the northern North Sea, however, the situation is more complicated in that the rotated mechanisms there,

contrary to what was claimed by Lindholm et al. (1995), are more scattered and also spatially more mixed with the others (Møllegaard 2000). This calls for a different explanation for the stress axis rotation, as compared to the Nordland region. We do not claim to have such an explanation, however, a satisfactory mechanism should be expected somehow to modify the stress tensor at a fault close to rupture. We are aware of two types of mechanism which may have such effects, one tied to Coulomb failure stress and the other to dilation effects.

The first one is that of intra-earthquake stress interac-tion, brought into attention following the 1992 M_W 7.3 Landers, California, earthquake, and investigated exten-sively after that. An earthquake can cause changes in shear and normal stress on surrounding faults, thereby affecting the seismicity rate there. The presence of such stress triggering mechanisms has been demonstrated already for many regions of the world, for larger earthquakes (for a recent review, see Stein 1999). Even though this concept never has been tested for low-seismicity areas such as the northern North Sea, the complex geology and the high density of capable faults is such that the possibility for intra-earthquake stress dependence is conceivable. Whether this also could explain the stress rotations is yet another unresolved question.

The other mechanism has been suggested recently by Nick Barton (pers. comm. 1999), based on the fact that dilation accompanying rock failure and weakness zone shearing introduces a component of shear strain that is no longer parallel to the assumed direction of shearing. In this case traditional Mohr theory may result in incorrect estimates of both the shear and normal components (Barton 1986), and may significantly affect the balance between the stress components. The normal and shear stress changes that accompany dilatant shearing can radically alter the principal stress components, thereby potentially rotating major principal stresses. We do not know, however, when such dilation effects could be expected to occur in the present setting.

References

Ask, M. V. S. 1988: In situ stress breakouts in the Danish sector of the North Sea. *Mar. Petr. Geol. 14,* 231–243.

Atakan, K., Lindholm, C. D. & Havskov, J. 1994: Earthquake swarm in Steigen, northern Norway: an unusual example of intraplate seismicity. *Terra Nova 6,* 180–194.

Barton, N. R. 1986: Deformation phenomena in jointed rock. *Géotechnique 36,* 147–167.

Bjørlykke, K. 1995: Fracturing and brittle/ductile properties of sedimentary rocks in relation to diagenesis and in situ stress. *In* Fejerskov, M. & Myrvang, A. M. (eds.), *Proceedings of the Workshop: Rock Stresses in the North Sea,* pp. 64–75. University of Trondheim, Norway.

Bjørlykke, K. & Høeg, K. 1997: Effects of burial diagenesis on stresses, compaction and fluid flow in sedimentary basins. *Mar. Petr. Geol. 14,* 267–276.

Bungum, H., Alsaker, A., Kvamme, L. B. & Hansen, R. A. 1991: Seismicity and seismotectonics of Norway and nearby continental shelf areas. *Journal of Geophysical Research 96,* 2249–2265.

Bungum, H. & Fyen, J. 1979: Hypocentral distribution, focal mechanisms and tectonic implications of Fennoscandian earthquakes, 1954–1978. *GFF 101,* 261–271.

Bungum, H., Hokland, B., Husebye, E. S. & Ringdal, F. 1979: An exceptional intraplate earthquake sequence in Meløy, northern Norway. *Nature 280,* 32–35.

Bungum, H. & Kristoffersen, Y. 1980: A microearthquake survey of the Svalbard region. *Final report, Phase I. NORSAR Tech. Rep. 1/80, NTNF/NORSAR, Kjeller, Norway,* 28

Bungum, H. & Lindholm, C. 1996: Seismo -and neotectonics in Finnmark, Kola and the southern Barents Sea. Part 2: Seismological analysis and seismotectonics. *Tectonophysics 270,* 15–28.

Byrkjeland, U., Bungum, H. & Eldholm, O. 2000: Seismotectonics of the Norwegian continental margin. *Journal of Geophysical Research 105,* 6221–6236.

Chan, W. W. & Mitchell, B. J. 1985: Intraplate earthquakes in northern Svalbard. *Tectonophysics 114,* 181–191.

Dehls, J., Olesen, O. 1998: NEONOR: Neotectonics in Norway: Annual technical report 1997, Rep. 98.016, 149 pp., Norges Geol. Undersøkelse, Trondheim.

Dehls, J. & Olesen, O. 1999: NEONOR: Neotectonics in Norway: Annual technical report 1998, Rep. 99.007, 206 pp., Norges Geol. Undersøkelse, Trondheim.

Dehls, J. & Olesen, O. 2000: NEONOR: Neotectonics in Norway: Final report, Rep. 2000.002, 119 pp., Norges Geol. Undersøkelse, Trondheim.

Fejerskov, M. & Lindholm, C. D. 2000: Crustal stress in and around Norway: an evaluation of stress generating mechanisms. *In* Nøttvedt, A. et al. (eds.): *Dynamics of the Norwegian Margin. Geol. Soc., London, Special Publications* 167, 441–449.

Fejerskov, M., Lindholm, C. D., Bungum, H., Myrvang, A., Bratli, R. K. & Larsen, B. T. 1996: Crustal stresses in Norway and adjacent offshore regions, Final report for the IBS-DNM project, topic 1.3 "Regional Stress Field", Norwegian Institute of Technology, Trondheim, Norway, 29.

Frolich, C. & Apperson, K. D. 1992: Earthquake focal mechanisms, moment tensors, and the consistency of seismic activity near plate boundaries. *Tectonics 11,* 279–296.

Gephart, J. W. & Forsyth, D. W. 1984: An improved method for determining the regional stress tensor using earthquake focal mechanism data: application to the San Fernando earthquake sequence. *Journal of Geophysical Research 89,* 9305–9320.

Gephart, J. W. 1990a: FMSI: A FORTRAN program for inverting fault/slickenside and earthquake focal mechanism data to obtain the regional stress tensor. *Computers & Geosciences 16,* 953–989.

Gephart, J. W. 1990b: Stress and the direction of slip of fault planes. *Tectonics 9,* 845–858.

Hansen, R. A., Bungum, H. & Alsaker, A. 1989: Three recent larger earthquakes offshore Norway. *Terra Nova 1,* 284–295.

Havskov, J. & Bungum, H. 1987: Source parameters for earthquakes in the Northern North Sea. *Norsk Geologisk Tidsskrift 67,* 51–58.

Herrmann, R. B. 1978: A note on causality problems in the numerical solution of elastic wave propagation in cylindrical coordinate systems. *Bulletin of the Seismological Society of America 68,* 117–124.

Herrmann, R. B. 1979: SH-wave generation by dislocation sources – a numerical study. *Bulletin of the Seismological Society of America 69,* 1–15.

Hicks, E. C. 1996: Crustal stresses in Norway and surrounding areas as derived from earthquake focal mechanism solutions and in situ stress measurements. Cand. Scient thesis, University of Oslo, Norway, 164 pp.

Hicks, E. C., Bungum, H. & Lindholm, C. D. 2000: Seismic activity, inferred crustal stresses and seismotectonics in the Rana region, Northern Norway. *Quaternary Science Reviews 19,* 1423–1436.

Kibsgaard, A. 1985: Focal mechanism studies of P to SV amplitude ratio. Cand. Scient thesis, University of Oslo, Norway, 115 pp.

Lazareva, A. P. & Misharina, L. A. 1965: Stresses in earthquake foci in the Arctic seismic belt. *Inv. Earth. Phys. Ser. 2,* 5–10 (translated)..

Lindholm, C. D., Bungum, H., Bratli, R. K., Aadnøy, B. S., Dahl, N., Tørudbakken, B. & Atakan, K. 1995: Crustal stress in the northern North Sea as inferred from in situ measurements and earthquake focal mechanisms. *Terra Nova 7,* 51–59.

Lindholm, C. D., Bungum, H., Hicks, E. & Villagran, M. 2000: Crustal stress and tectonics in Norwegian regions determined from earthquake focal mechanisms. *In* Nøttvedt, A. et al. (eds.): *Dynamics of the Norwegian Margin. Geol. Soc., London, Special Publications* 167, 429–439.

Lindholm, C. D. & Havskov, J. 1989: Final report on evaluation of Statfjord OBS data. A detailed study of the seismicity in northern North Sea. *Progress Report No. 11, Institute of Solid Earth Physics, University of Bergen, Norway,* 34 pp.

Lund, B. & Slunga, R. 1999: Stress tensor inversion using detailed microearthquake information and stability contraints: application to Ölfus in southwest Iceland. *Journal of Geophysical Research 104,* 14947–14964.

Mitchell, B. J., Bungum, H., Chan, W. W. & Mitchell, P. B. 1990: Seismicity and present-day tectonics of Svalbard. *Geophysics Journal International 102,* 139–149.

Møllegaard, E. 2000 *Seismotektonikk i nordlige Nordsjø. Cand. scient thesis, University of Oslo,* 172 pp.

Muir Wood, R. 1989: The Scandinavian earthquakes os 22 December 1759 and 31 August 1819. *Disasters 12,* 223–236.

NORSAR and NGI 1998: Seismic Zonation for Norway, Rep., 188 pp., Norwegian Council for Building Standardization (NBR), Oslo.

Olesen, O. 1988: The Stuoragurra fault, evidence of neotectonics in the Precambrian of Finnmark, northern Norway. *Norsk Geologisk Tidsskrift 68,* 107–118.

Parker, R. L. & McNutt, M. K. 1980: Statistics for the One-Norm Misfit Measure. *Journal of Geophysical Research 85,* 4429–4430.

Savostin, L. A. & Karasik, A. M. 1981: Recent plate tectonics of the Arctic basin and of northeastern Asia. *Tectonophysics 74,* 111–145.

Slunga, R. 1981: Fault mechanisms of Fennoscandian earthquakes and regional crustal stresses. *Geol. För. Stockh. Förh. 103,* 27–31.

Stein, R. S. 1999: The role of stress transfer in earthquake occurrence. *Nature 402,* 605–609.

Stein, S., Cloetingh, S., Sleep, N. H. & Wortel, R. 1979: Passive margin earthquakes, stresses and rheology. *In* Gregersen, S. & Basham, P. W. (eds.): *Earthquakes at North-Atlantic Passive Margins: Neotectonics and Postglacial Rebound,* NATO ASI Ser., 266, 231–259.

Vaage, S. 1980: Seismic evidence of complex tectonics in the Meløy earthquake area. *Norsk Geologisk Tidsskrift 60,* 213–217.

Wang, C. E. & Herrmann, R. B. 1980: A numerical study of P-, SV-, and SH-wave generation in a plane layered medium. *Bulletin of the Seismological Society of America 70,* 1015–1036.

Zoback, M. L. 1992: First and second-order lithospheric stress patterns. *Journal of Geophysical Research 97,* 11703–11728.